Impact of strain on electronic defects in (Mg,Zn)O thin films

Florian Schmidt, Stefan Müller, Holger von Wenckstern, Gabriele Benndorf, Rainer Pickenhain, and Marius Grundmann

Citation: Journal of Applied Physics **116**, 103703 (2014); doi: 10.1063/1.4894841
View online: https://doi.org/10.1063/1.4894841
View Table of Contents: http://aip.scitation.org/toc/jap/116/10
Published by the American Institute of Physics

Impact of strain on electronic defects in (Mg,Zn)O thin films

Florian Schmidt,[a] Stefan Müller, Holger von Wenckstern, Gabriele Benndorf, Rainer Pickenhain, and Marius Grundmann
Universität Leipzig, Institut für Experimentelle Physik II, Linnéstraße 5, 04103 Leipzig, Germany

(Received 23 July 2014; accepted 26 August 2014; published online 8 September 2014)

We have investigated the impact of strain on the incorporation and the properties of extended and point defects in (Mg,Zn)O thin films by means of photoluminescence, X-ray diffraction, deep-level transient spectroscopy (DLTS), and deep-level optical spectroscopy. The recombination line Y_2, previously detected in ZnO thin films grown on an Al-doped ZnO buffer layer and attributed to tensile strain, was exclusively found in (Mg,Zn)O samples being under tensile strain and is absent in relaxed or compressively strained thin films. Furthermore a structural defect E3′ can be detected via DLTS measurements and is only incorporated in tensile strained samples. Finally it is shown that the omnipresent deep-level E3 in ZnO can only be optically recharged in relaxed ZnO samples.
 [http://dx.doi.org/10.1063/1.4894841]

I. INTRODUCTION

Wide bandgap semiconductors have gained importance and have become technologically relevant in applications such as blue light emitting diodes, UV photo-detectors, high power devices or transparent electronics. Besides the well established nitrides,[1,2] oxides like indium oxide, tin oxide[3–5] or zinc oxide[6,7] (ZnO) triggered research on transparent conducting oxides as new field of material science. In recent years the semiconducting properties of such oxides were exploited, however, the difficulties concerning *p*-type doping have restricted research to unipolar devices, especially transistors to be utilized in transparent electronics.[8,9] Concerning transistors, heterostructures enable fabrication of high-electron mobility transistors but also for the study of confinement effects in quantum wells (QWs) heterostructures are essential. For the case of ZnO magnesium is commonly used for bandgap engineering and realization of QWs. Piezoelectric polarization induced by the strain within the heterostructure modifies recombination properties.[10] Further, strain is often accommodated by the incorporation of extended defects. Polarization-induced changes of recombination properties of QWs is not an issue for non-polar samples,[11–16] however, strain-induced defects are also of importance for such layers. It was shown before that strain influences the recombination properties of ZnO thin films.[17] In this contribution, we investigate the impact of in-plane strain on (i) the incorporation of extended defects in (Mg,Zn)O and (ii) the modification of defect properties.

II. SAMPLES

(Mg,Zn)O thin films having a thickness of approximately 1 μm were grown by pulsed-laser deposition (PLD) on $10 \times 10\,\text{mm}^2$ *a*-plane and *r*-plane sapphire substrates, respectively. For that a growth temperature of approximately 650 °C and an oxygen pressure of 0.016 mbar were used. A detailed description of the PLD growth setup can be found in Ref. 18. The respective ceramic MgO/ZnO targets used for sample growth have admixtures of no, 0.10 wt. %, 0.25 wt. %, 1.00 wt. %, and 2.00 wt. % MgO. The Mg-content in the thin films was estimated via low temperature photoluminescence (PL) by evaluating the bandgap shift determined from the energetic position of the I_6-line,[19] as it is described in Ref. 20 and summarized in Table I. Prior to the ZnO layer, an about 200 nm thick aluminium doped (1 wt. %) ZnO (AZO) layer was deposited, which serves as ohmic back-contact and leads to low series resistance of the Schottky diode.[21] The high Al-content within this functional layer leads to an increase of the *a*- and a decrease of the *c*-lattice compared to nominally undoped ZnO.[22,23] A schematic picture of the structure is shown in Fig. 3(b). Schottky contacts were realized by reactive dc-sputtering of PdO_y with a subsequent capping with metallic palladium.[24] All samples were mounted on sockets having a hole in their center in order to facilitate the illumination from the backside of the structure.

III. RECOMBINATION

PL measurements have been carried out in a helium-bath cryostat at $T = 2\,\text{K}$. The samples were excited with an excitation density of about $2\,\text{W/cm}^2$ using the 325 nm line of a He-Cd laser. The sample luminescence was spectrally dispersed by a monochromator with a focal length of

TABLE I. Target- and thin film-composition and energetic position of the I_6-line. The Mg-content of the thin films was obtained via Eq. (1) from Ref. 20.

Target composition	E_{I_6} (e V)	Film composition
0.00%	3.3596	0.0%
0.10%	3.363	0.2%
0.25%	3.369	0.5%
0.50%	3.375	0.8%
1.00%	3.404	2.2%
2.00%	3.450	4.6%

[a]Electronic mail: fschmidt@physik.uni-leipzig.de

$f = 320$ mm using a 2400 grooves/mm grating and detected by a Peltier-cooled GaAs photomultiplier.

For (Mg,Zn)O the binary end components, ZnO and MgO, have a wurtzite and a rocksalt crystal structure, respectively. The $Mg_xZn_{1-x}O$ alloy shows a transition from one structure to the other at a concentrations of $0.5 < x < 0.6$. Empirically, for the wurtzite phase of the alloy the c-lattice constant decreases while the a-lattice constant increases with respect to binary ZnO.[25–27] The cell volume of the wurtzite phase $\propto ca^2$ depends very little on the Mg concentration and thus gives reason to the antagonistic behavior[27] with $\partial c/\partial x \approx -2\partial a/\partial x$. The change of the binding length of the an- and cation leads to a change in the size of the band gap, which then depends on the composition. Alloying ZnO by MgO will increase the fundamental bandgap compared to binary ZnO.[28,29] The Mg-content was estimated via Eq. (1) from Ref. 20 by using the energetic position of the I_6-line

$$E_{I_6} = 3.3601(7)\,\text{eV} + 1.96(2)\,\text{eV} \times x. \quad (1)$$

For the current study the alloying of ZnO with MgO allows to tune the strain state of polar (Mg,Zn)O thin films on the ZnO:Al buffer layer. For binary ZnO and for low Mg-contents the polar thin films are expected to be under tensile in-plane strain.[22,23] But if the Mg-content is increased more and more there will be a critical Mg concentration x_c for which the AZO buffer and the (Mg,Zn)O thin film have similar a-lattice constant. If the Mg-content is increased above x_c the (Mg,Zn)O layers grow relaxed. In Fig. 1, we have compiled the PL data such that the energy scale starts at the transition energy of the I_6 defect or in other words, the energy scale is shifted such that the I_6 transition lies at $E = 0$ eV for each Mg-content. This is done in order to allow direct comparison of PL features of the investigated samples. In this representation, it is easily seen that the Y_0-line is present in all samples.[19] In an alloy, the random distribution of atoms causes a significant inhomogeneous broadening effect of luminescence lines, which is called *alloy broadening*.[30–32] In particular, for (Mg,Zn)O system alloy broadening has been discussed in Refs. 33–35. Therefore, the full-width at half maximum (FWHM) increases for higher Mg-contents. For the sample with highest Mg-content the Y_0-line is due to alloy broadening hardly visible. Further, on the energy scale chosen it red-shifts for higher Mg-content due to the increasing band-gap with increasing Mg-content. The structural defect-bound excitonic recombination Y_2 (Ref. 36) is not present for the samples with a Mg-content of $x \geq 0.8\%$. Brandt *et al.* recently showed that this line is connected to tensile strain in ZnO layers.[17] From the representation chosen in Fig. 1, it is evident that it is not the alloy broadening that hinders the resolution of this peak; this feature is absent for the three samples with highest Mg-content. For the samples with a Mg-content of $x \leq 0.5\%$ and, of course, for binary ZnO the Y_2-line is clearly visible. Relying on the fact that the appearance of the Y_2-line is connected to tensile strain in the layer and recalling that here the in-plane a-lattice constant increases in (Mg,Zn)O with increasing Mg-content we argue that the binary ZnO layer and the layers with a Mg-content up to 0.5% are under tensile strain. For Mg-contents of 0.8% and higher the in-plane a-lattice constant of the (Mg,Zn)O-layer is greater or equal to that of the ZnO:Al buffer layer. Please note, that Brandt *et al.* changed the buffer layer in order to change the strain state of the sample. In case of the ternary (Mg,Zn)O thin films, we however control the lattice constant of the thin film itself by changing the Mg-content. In both cases tensile strain introduces an extended defect traceable by the occurrence of the Y_2 excitonic recombination.[36]

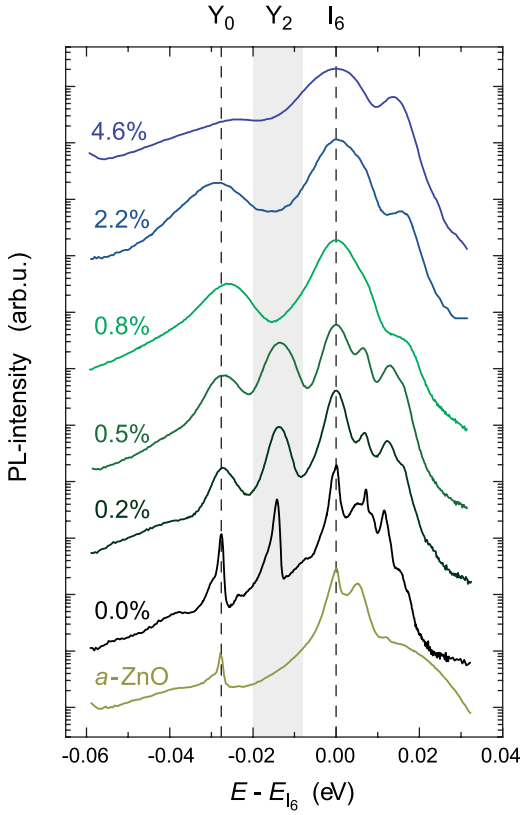

FIG. 1. Low-temperature photoluminescence spectra ($T = 2$ K) of an a-oriented ZnO thin film grown on r-sapphire and six c-oriented (Mg,Zn)O alloys with $0 \leq x \leq 4.6\%$ as labeled grown on a-sapphire, respectively. The lines have been shifted for clarity in vertical and horizontal direction, as described in the text.

Low temperature photoluminescence measurements of binary polar (c-ZnO) and non-polar (a-ZnO) ZnO thin films are depicted in Fig. 1 as well. While the luminescence feature Y_0 is visible independent of the growth direction, Y_2 does not occur for the non-polar thin film but is quite prominent for the polar ZnO sample as mentioned before.

IV. STRUCTURAL PROPERTIES

The lattice constants were obtained by means of X-ray diffraction (XRD) using a PANalytical X'Pert Pro diffractometer. Figure 2(a) depicts the wide angle XRD scans of all thin film samples. Substrate peaks occurring at angles of 37.8° and 80.8° correspond to the (11.0) and (22.0) planes of the a-plane sapphire and at 25.7°, 52.6°, and 83.4° correspond to the (01.2), (02.4), and (03.6) planes of the r-plane sapphire, respectively. The peaks visible at 34.4° and 72.6° are the (00.2) and (00.4) reflections of the c-oriented (Mg,Zn)O samples, respectively. The reflex of the (11.0)

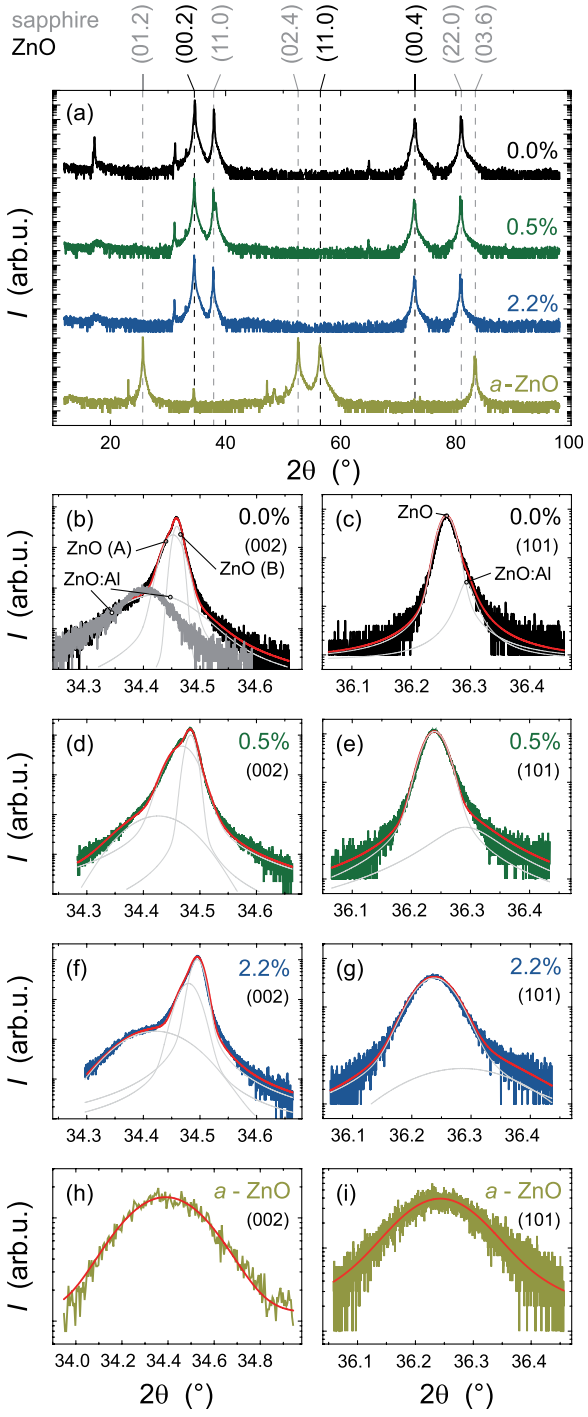

FIG. 2. (a) wide angle 2θ-ω scans and (b) to (i) scans of the (00.2)- and (10.1)-reflex of an *a*-oriented ZnO thin film and three *c*-oriented (Mg,Zn)O alloys with $x = 0$, 0.5%, and 2.2%. The red lines correspond to fits of the data assuming Voigt-curves.

plane of the non-polar ZnO thin film occurs at 56.5°. The positions of the (00.2)- and (10.1)-reflexes were evaluated by fitting the data assuming Voigt profiles. The 2θ-ω scans are shown in Fig. 2, in which the fitted curves are shown as red solid lines, respectively. The calculated lattice constants are summarized in Table II.

Thin films grown on *a*-plane saphire substrates are *c*-orientated with their *a*-lattice constants lying parallel and their *c*-lattice constants lying perpendicular to the *c*-oriented AZO buffer layer. The (Mg,Zn)O films were grown on an AZO buffer layer, the (00.2)-peak of such a layer is shown for comparison in Fig. 2(b) as a grey line and yields a *c*-axis lattice parameter of 5.2096 Å. The (10.1)-reflex is rather broad leading to a high inaccuracy in the *a*-lattice constant, which amounts to 3.2481 Å.

For the polar *c*-oriented (Mg,Zn)O films the lineshape of the XRD peaks is asymmetric and reveals 3 contributions for the (00.2)-peaks and 2 underlying signals for the (10.1)-reflexes. The broad tail of the (00.2)-peak at lower angles is due to the AZO buffer layer, which is in accordance with the XRD measurement of the 200 nm thick AZO reference sample (grey line in Fig. 2(b)). This back-contact layer is also visible at higher 2θ-angles for the (10.1)-peaks, respectively. Furthermore, all (00.2)-peaks of the polar samples show a shoulder at lower angles. The corresponding XRD-peak is labelled with "A," the main part of the signal with "B" in Fig. 2(b). Since lower angles in the (00.2)-scan correspond to higher *c*-lattice constants, part A of the signal is related to a region A of the sample, which is more influenced by the underlying AZO buffer layer, as depicted in Fig. 3(c). Due to, e.g., dislocations the strain is reduced in the (larger) region B, which is responsible for the lion's share of the XRD signal. This is the region probed by PL and by the space charge spectroscopic methods deep-level transient spectroscopy[37] (DLTS) and deep-level optical spectroscopy[38–40] (DLOS), shown in Secs. V and VI. The increase of the Mg-content in (Mg,Zn)O leads to an decrease of the *c*-lattice constant while the *a*-lattice constant increases.

In Fig. 3(a) the *a*- and *c*-lattice constants for all (Mg,Zn)O samples are compared. The open symbols represent lattice constants obtained from region A of the sample, while the solid marks show the corresponding constants obtained from region B (cmp. Fig. 3(b)). The *a*-lattice constant of the 200 nm thick AZO layer is higher compared to that of binary ZnO (Ref. 23) leading to tensile strain in those films. An increase of the Mg-content x reduces the tensile strain until the films grow unstrained on the AZO buffer, a further increase of x leads to relaxation of the thin films. From Fig. 3(b) a change in the strain state can be expected between $0.5\% < x < 0.8\%$. Remarkably the samples with $0.0\% \leq x \leq 0.5\%$ and $x \geq 2.2\%$, i.e., before and after this transition, show the same slope in *a* over *c*, which is indicated by the dashed line in Fig. 3(b).

The situation is different in the *a*-oriented non-polar ZnO thin film, where the *c*-lattice and one *a*-lattice constant ($a_{\parallel}$) are lying in the (11.0)-plane, as shown in Fig. 3(d). The in-plane lattice constants are calculated from the positions of the (00.2)- (c) and (11.0)-reflex ($a_{\parallel}$), respectively. The out-of-plane *a*-lattice constant ($a_{\perp}$) was obtained via the position of the (10.0)-peak. The in-plane *c*-lattice constant is smaller than the bulk value indicating uniaxial in-plane compressive strain, which is also manifested in the blue-shift of the I_6 transition by 1 meV (not shown). Therefore, the out-of-plane $a_{\perp}$-lattice constant is higher than the bulk value in order to maintain the unit cell volume, as illustrated in Fig. 3(d), where the wire frame model depicts the dimension of the polar ZnO thin film.

The observed values for the in- and out-of-plane lattice constants and the associated strain of the films are confirmed

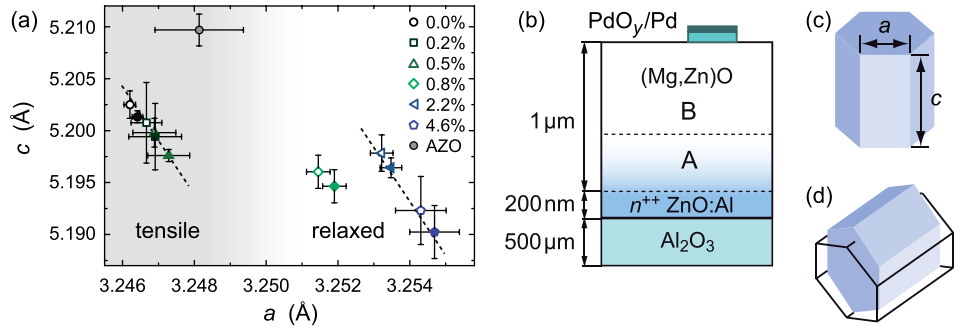

FIG. 3. (a) *a*- and *c*-lattice constants of the *c*-(Mg,Zn)O thin films and an AZO buffer reference obtained from XRD scans as shown in Fig. 2. Open (solid) symbols represent the lattice constants streaming from region A (region B), as illustrated in (b). (b) Schematic depiction of the sample-structure investigated with a thin film layer consisting of two regions A and B, and an underlying highly conducting AZO buffer layer. (c) and (d) illustration of an unit-cell of *c*- and *a*-oriented ZnO, respectively. The wire frame model in (d) represents the dimension of the *c*-ZnO unit cell shown in (c).

by the results obtained from the PL experiments, here the Y_2-line is absent in samples which are not under tensile strain.

V. DEEP DEFECTS

Prior to the DLTS studies the net doping density N_{net} was determined from capacitance-voltage measurements (*CV*) conducted at room temperature using an Agilent 4294 A capacitance bridge. Therefore, a probing frequency of 1 MHz was applied. N_{net} lies in the range of $10^{17}\,cm^{-3}$, the corresponding values are listed in Table III.

Defects with electronic states in the upper third of the ZnO band gap were studied by DLTS in the temperature range from 10 K to 330 K using a helium flow cryostat. A description of the DLTS setup can be found in Ref. 41. For the measurements a probing frequency of 1 MHz was used. The samples were biased at $V = -3$ V and excited with filling pulses of 3.5 V having a length of $t_p = 1$ ms. Such pulses almost flattened the bands and ensure a complete filling of the incorporated deep levels. Rate windows in the range of 2.5 Hz to 1000 Hz were applied. The DLTS scans are shown in Fig. 4 for the *a*-oriented ZnO sample as well as the *c*-oriented (Mg,Zn)O thin films with Mg-contents as labelled. For that a rate-window of 500 Hz was applied.

The measurements reveal peaks corresponding to deep levels commonly observed in PLD grown thin films, such as T1,[42–44] E64,[45] E1,[46–50] T2,[51–61] E3,[46,50,52,55–58,62–67] E3′,[57,68] and E4.[49,56,57,64,66] The trap parameters, i.e., the thermal activation energy E_t and the apparent capture cross-section σ_n, as well as the trap concentrations N_t of the defects are collected in Table III. The error bars shown were obtained from the slope of the linear fits of the Arrhenius representations, respectively. We note that the apparent capture cross-section of the E4 defect is for the non-polar sample by two orders of magnitude smaller compared to the polar sample, but further discussion of this issue is beyond the scope of this work. The defect E3 was detected in all samples independent of orientation and Mg-content of the thin films. A peak at about 60 K corresponds to the deep-level E1 and was found in all *c*–(Mg,Zn)O samples. While contributions of the deep-levels T1, E64, and T2 are only detectable in *c*–(Mg,Zn)O samples with $x \leq 0.5\%$, the signals of these defects lie below the detection limit in samples with $x \geq 0.8\%$. The E3 concentration, on the other hand, tends to increase with increasing Mg-content in latter samples. Since there is no dependence of the net-doping density on *x*, no change of the Fermi-level position is supposed. Therefore, we conclude that T1, E64, T2, and E4 are actually not incorporated in these samples. A notable decrease of the signal-to-noise ratio is observed in the (Mg,Zn)O sample with $x = 0.8\%$.

By using high-resolution Laplace-DLTS[69,70] (LDLTS), Auret *et al.* revealed that a defect labeled E3′ exists in as-grown ZnO thin films on AZO buffer causing a DLTS signal in the vicinity of that of E3.[57] In a conventional DLTS scan E3′ usually occurs only as a shoulder on the high temperature side of the E3 peak for higher rate-windows the signals

TABLE II. Lattice constants and FWHM ($\Delta\omega_{FMHW}$) values of the *c*-oriented (Mg,Zn)O and *a*-oriented ZnO thin films obtained from XRD scans. The corresponding region "A" and "B" are shown in Fig. 3(b), respectively. The FWHM was obtained from rocking-curves of the (00.2)-reflex for the polar *c*-oriented (Mg,Zn)O films and of the (11.0)-reflex for the *a*-oriented ZnO sample.

Material	Mg-content (%)	a_A (Å)	c_A (Å)	a_B (Å)	c_B (Å)	$\Delta\omega_{FMHW}$ (°)
c-ZnO:Al (AZO)	–	3.2481(12)	5.2096(15)	–	–	
c-ZnO	0.0	3.2462(2)	5.2025(13)	3.2464(2)	5.2013(6)	0.08
c-(Mg,Zn)O	0.2	3.2467(4)	5.2008(39)	3.2469(7)	5.1994(32)	0.12
c-(Mg,Zn)O	0.5	3.2469(7)	5.1998(13)	3.2473(6)	5.1976(6)	0.10
c-(Mg,Zn)O	0.8	3.2515(3)	5.1960(16)	3.2519(3)	5.1947(16)	0.17
c-(Mg,Zn)O	2.2	3.2532(3)	5.1978(18)	3.2535(3)	5.1964(9)	0.15
c-(Mg,Zn)O	4.6	3.2543(7)	5.1923(33)	3.2547(7)	5.1902(26)	0.13
a-ZnO	–	($a_{\parallel}$) 3.2439(130) ($a_{\perp}$) 3.2595(94)	5.1904(447)	–	–	0.61

TABLE III. Trap parameters (thermal activation energy E_t, apparent capture cross-section σ_n) and defect concentrations N_t obtained from DLTS, LR-DLTS (LR) and LDLTS ($\mathcal{L}$) experiments.

			c-(Mg,Zn)O					
		a-ZnO	0.0%	0.2%	0.5%	0.8%	2.2%	4.6%
	N_{net} (10^{16} cm^{-3})	6.7	13.3	21.1	17.5	24.3	30.7	19.3
T1	E_t (meV)	–	25(7)	–	27(4)	–	–	–
	σ_n (10^{-15} cm^2)	–	4.4(24)	–	1.5(26)	–	–	–
	N_t (10^{14} cm^{-3})	–	4.5	–	1.7	–	–	–
E64	E_t (meV)	–	87(2)	82(8)	80(5)	–	–	–
	σ_n (10^{-1} cm^2)	–	9.3(25)	3.4(19)	1.4(22)	–	–	–
	N_t (10^{14} cm^{-3})	–	3.1	2.6	3.5	–	–	–
E1	E_t (meV)	–	113(3)	115(6)	123(3)	107(10)	108(8)	126(7)
	σ_n (10^{-13} cm^2)	–	0.9(7)	1.0(7)	2.2(13)	0.7(15)	1.2(20)	3.3(18)
	N_t (10^{15} cm^{-3})	–	1.7	1.4	2.3	0.7	0.6	1.8
T2	E_t (meV)	–	266(7)	223(9)	251(13)	–	–	–
	σ_n (10^{-14} cm^2)	–	3.8(31)	0.4(26)	1.2(41)	–	–	–
	N_t (10^{14} cm^{-3})	–	4.4	6.5	8.0	–	–	–
E3 (LR)	E_t (meV)	–	291(5)	305(9)	316(6)	307(9)	319(7)	358(10)
	σ_n (10^{-16} cm^2)	–	3.6(16)	3.1(23)	9.8(17)	5.1(31)	6.2(27)	16.2(44)
	N_t (10^{15} cm^{-3})	–	5.9	2.6	2.2	3.4	22.4	25.9
E3($\mathcal{L}$)	E_t (meV)	307(8)	295(8)	287(4)	321(11)	308(6)	316(14)	365(6)
	σ_n (10^{-16} cm^2)	6.3(36)	4.3(13)	2.3(16)	12.7(21)	6.9(27)	3.7(18)	13.1(39)
	N_t (10^{15} cm^{-3})	3.5	2.5	1.6	1.5	3.1	23.9	22.7
E3′ ($\mathcal{L}$)	E_t (meV)	–	380(4)	372(12)	370(19)	–	–	–
	σ_n (10^{-14} cm^2)	–	2.6(20)	1.1(14)	1.0(17)	–	–	–
	N_t (10^{15} cm^{-3})	–	3.8	1.1	0.9	–	–	–
E4	E_t (meV)	562(67)	–	–	503(41)	–	–	–
	σ_n (10^{-15} cm^2)	0.3(4)	–	–	38(21)	–	–	–
	N_t (10^{14} cm^{-3})	1.8	–	–	2.5	–	–	–

of E3 and E3′ merge making the determination of the individual DLTS maxima difficult if not impossible. In order to investigate these defects unambiguously, two approaches were pursued:

1. A low-rate DLTS (LR-DLTS) setup[68] was used in order to extend the applicable rate-windows to the mHz regime. For such rate-windows the DLTS peaks of E3 and E3′ are shifted to lower temperatures at which the emission rate of E3 and E3′, respectively, and with that the DLTS signals are easily distinguishable. On the basis of the LR-DLTS data an Arrhenius plot can be constructed.
2. High-resolution LDLTS[69,70] was applied for all samples of this study, as described in the following.

In Fig. 5, LDLTS spectra calculated from isothermal capacitance transients recorded at $T = 180$ K are shown. It turns out that the signal of E3′ is only detectable in samples with a Mg-content of $x \leq 0.5\%$, which are under tensile strain. It is absent in the relaxed polar (Mg,Zn)O samples with $x \geq 0.8\%$ and in the compressively strained non-polar *a*-ZnO film. The E3′ defect shows a strong dependence on filling pulse duration and temperature, which is often associated with a defect that has a capture barrier for carrier capture. Auret *et al.* investigated the carrier capture of E3′ and concluded that E3′ "is not a well-defined point defect but […] it may have a somewhat extended nature onto which multiple charges can be captured, thus leading to a Coulomb barrier, somewhat like carrier capture onto a dislocation."[57] Furthermore the authors found that E3′ "is most prevalent in as-grown samples and samples that had been annealed in an oxygen atmosphere, suggesting that E3′ may be related to oxygen incorporation in the lattice."[57] The idea of E3′ being an extended defect goes along with the fact that it is only incorporated in tensile strained films grown on an AZO buffer layer, which in turn introduces structural defects like dislocations in the film.

Regarding the positions of E1 and E3 in Fig. 4 in dependence of the Mg-content, it attracts attention that the peak maximum of E1 occurs almost at the same temperature independent of x, while a shift to higher temperatures is visible for the peak position of E3 in the (Mg,Zn)O samples with increasing x. That implies that the emission rate of E1 is independent of the Mg-content and that of E3 decreases with increasing Mg-content, which corresponds to an increase of the thermal activation energy of E3. The reason for that is the increase of the fundamental bandgap of (Mg,Zn)O with increasing x and the relative energetic difference between E1 and E3, respectively, with respect to E_c. Figure 6 shows the change of the energetic position $\Delta E_t := E_{t,x} - E_{t,x=0}$ of the defects E1 and E3, respectively, versus x. In the case of E3, the data were obtained from LR-DLTS measurements (solid circles) and LDLTS measurements (open circles, Fig. 5) to distinguish the signature of E3 and E3′ and avoid the determination of erroneous trap parameters. For E1, E_t and σ_n was obtained via the conventional DLTS measurement shown in Fig. 4. The change of the bandgap energy is given by the slope of $E_{I_6}(x)$ from Eq. (1) and indicated in Fig. 6 by the black solid line. The dashed

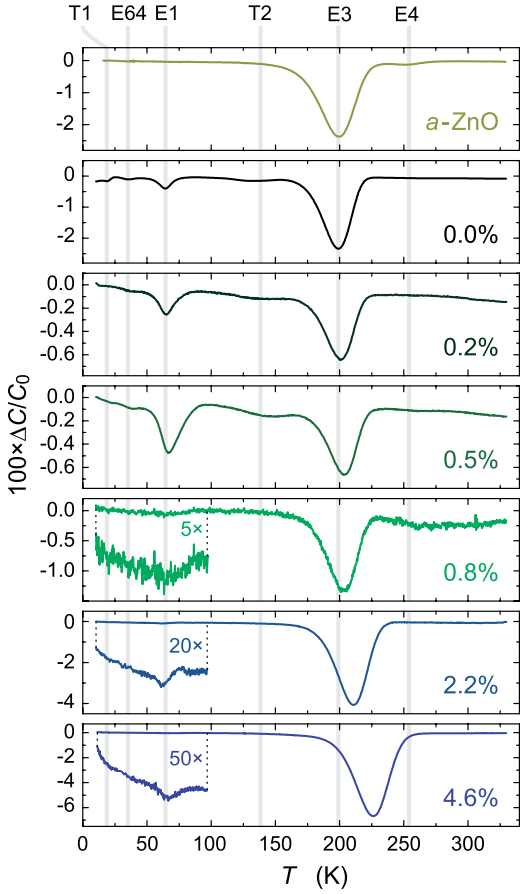

FIG. 4. DLTS scans of polar (Mg,Zn)O thin films with $0 \le x \le 4.6\%$ and a non-polar ZnO film for a rate-window of 500 Hz.

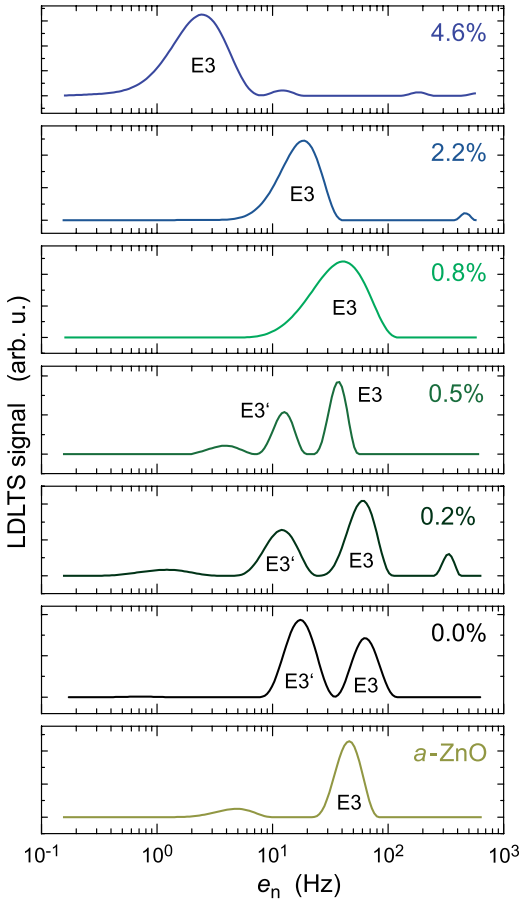

FIG. 5. LDLTS spectra of the *a*-ZnO and *c*-(Mg,Zn)O thin film samples, respectively, calculated from isothermal capacitance transients recorded at $T = 180$ K.

lines represent the linear fits of $\Delta E_{t,E1}$ and $\Delta E_{t,E3}$ vs. x, respectively. While ΔE_t increases with x for the defect E3, this value remains almost constant for E1. This is equivalent to an increase of the energetic distance of E_c and E_t for E3, while this spacing remains stable for E1. The increasing bandgap energy splits into a shift of the conduction band-edge ΔE_c and valence band-edge ΔE_v. The ratio of ΔE_c to ΔE_v amounts[26,71,72] $\Delta E_c/\Delta E_v = 0.9/0.1$ to 0.6/0.4. Rao *et al.* even report a negligible shift of the valence band[73] (and therefore, $\Delta E_g = \Delta E_c$). According to the literature, the corresponding range of ΔE_c is shaded in Fig. 6. Hence, the energetic position of E3 is fixed in the band and does not change with respect to the vacuum level, the change of E_c increases the thermal activation energy of the deep-level. E1, in contrast, shows only a minor change of its energetic position with respect to the conduction band-edge–the defect-level follows E_c. The electronic wavefunctions of E1 are with that predominantly derived from the conduction band which is not the case for the E3 defect.

VI. E3 IN STRAINED (Mg,Zn)O THIN FILMS

As shown in Secs. III–V, the Mg-content influences the kind of strain as well as incorporation of defects in (Mg,Zn)O thin films grown on a AZO buffer layer. In the following, the response of E3 on the optical excitation with infrared (IR) light is investigated. Therefore, we compare the results of a tensile strained (Mg,Zn)O thin film with $x = 0.5\%$ and a similar sample with $x = 2.2\%$ being relaxed.

DLTS measurements under dark conditions and under optical excitation[38,39] (DLOS) by the use of an IR laser were performed in a temperature range between 100 K and 200 K, respectively. We note that in the original work of Chantre *et al.* the method called DLOS[38] considers only the initial derivation of the capacitance transient ($t \to 0$) to obtain the

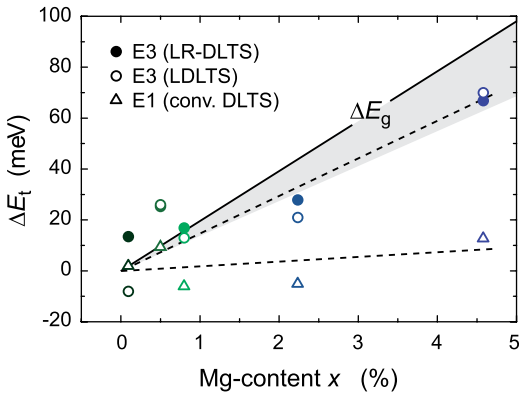

FIG. 6. Change in thermal activation energy ΔE_t of the deep-levels E1 (triangles) and E3 (circles), respectively, over Mg content x. The data were obtained from LDLTS (open symbols) and LR-DLTS experiments (solid symbols). The shaded area represents the change of the conduction band-edge ΔE_c reported in the literature.

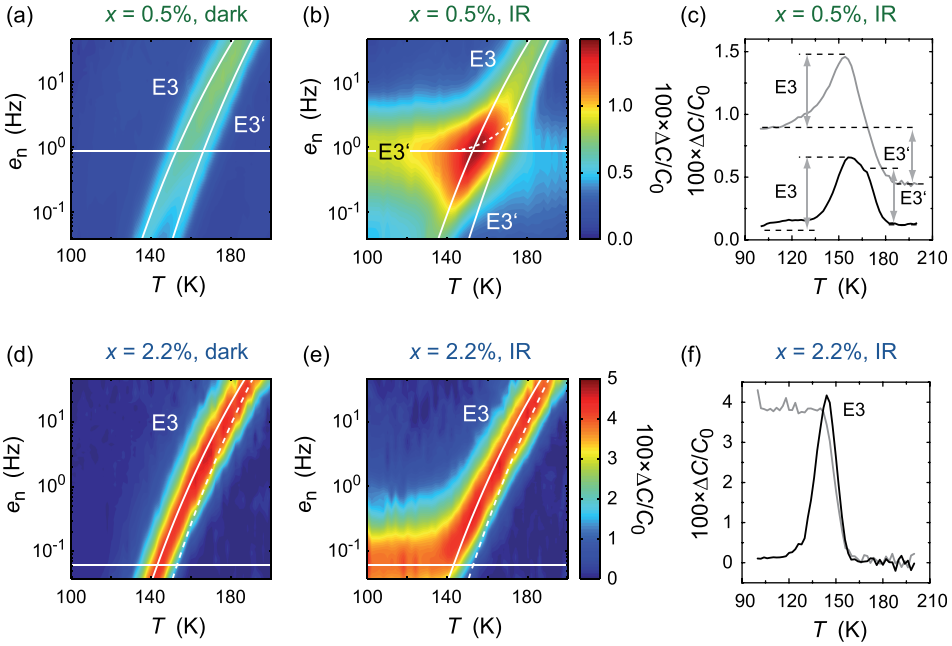

FIG. 7. DLTS scans ((a), (d)) and DLOS scans ((b), (e)) excited with photons of an IR laser. A comparison of measurements under dark condition and IR illumination for the emission rates indicated by the horizontal lines is shown in (c) and (f), respectively.

time constant τ. In this work, τ is obtained by folding the photo-capacitance transient with a lock-in correlation function as it is, in principle, done in Lang's conventional (thermal) DLTS[37] and as it was proposed by Brehme and Pickenhain.[74] However, nowadays it has been adopted to call an experiment deep-level optical spectroscopy in which isothermal capacitance transients following a voltage pulse to a *pn*- or Schottky-diode are recorded as a function of the energy of monochromatic light being incident on the diode. This is done regardless of the method used for extracting the time constant. Photons used in the DLOS experiment having a wavelength of 1064 nm ($E_{ph} = 1.17$ eV) are able to excite deep-levels with $E_t < 1.17$ eV, hence it is possible to recharge E3 and E3′ but not the midgap level T4,[75] which has an activation energy above the photon energy E_{ph}. The results for the tensile strained (Mg,Zn)O thin film are shown in Figs. 7(a)–7(c) and data obtained from the relaxed sample are depicted in (d)–(f), respectively. In Fig. 7(a), the thermal emission of the deep defects E3 and E3′ can be seen as highlighted by the solid lines, which represent the calculated values of the emission rate using the trap parameters obtained from LDLTS measurements as listed in Table III. While the signatures of E3 and E3′ can be resolved for low temperatures the DLTS signals merge for higher temperatures and appear as one single peak.

Under optical excitation a DLTS maximum between 100 K and 140 K can be found at about 1 Hz, which is independent of temperature and disappears after thermal emission of the defects, i.e., between 160 K and 200 K. The whole signal shows an offset due to contributions of deeper defects with $E_t < E_{ph}$, such as E4 and E5.[56,76]

In Fig. 7(c), DLTS scans using similar rate-windows, i.e., emission rates, are shown under dark condition (black line) and under optical excitation (grey line) for comparison as indicated by the horizontal line. Even though the concentrations of E3 and E3′ do not differ much, the step height occurring in the temperature scan between 120 K and 160 K with optical excitation can be assigned to E3′ and not E3. That means E3′ can be emptied optically with an optical emission rate e_n^o of approximately 1 Hz, whereas E3 cannot be recharged. The measurement of the relaxed (Mg,Zn)O thin film with $x = 2.2\%$ is shown in Fig. 7(d) to 7(f). It was shown by the LDLTS experiments that E3′ is not incorporated in such thin films. In contrast to the situation in the tensile strained sample, E3 can be recharged with $e_n^o \approx 100$ mHz, which we tentatively explain by means of an energy diagram as shown schematically in Fig. 8. From this depiction, it is evident that the interaction of E3 with the conduction band E_c depends on the strain state of the crystal and with that on the displacement of the E3-parabola with respect to the reciprocal coordinate Q. While E3 can be optical recharged in material being relaxed, the photo-ionization energy of E3 is larger in the tensile strained crystals leading to a much lower optical emission rate. Due to the latter the transition is not detectable within the measurement range probed in the experiments. Of course the thermal activation energy of E3 (as obtained from DLTS) is the same in both cases.

VII. SUMMARY

We investigated PLD grown (Mg,Zn)O thin films with Mg-contents between $0 \le x \le 4.6\%$ by means of PL, XRD, DLTS, LDLTS, LR-DLTS, and DLOS. Films were grown on a degenerately Al-doped ZnO buffer layer. Due to the Al doping, the *a*-lattice constant (*c*-lattice constant) is larger

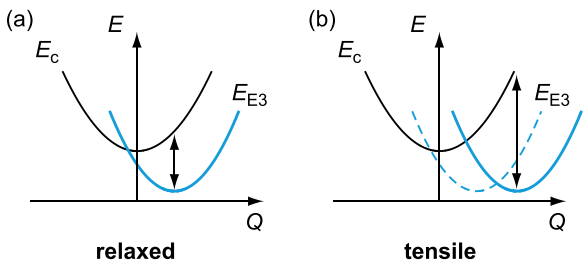

FIG. 8. Schematic illustration of an energy diagram of (a) relaxed and (b) tensile strained ZnO material, respectively, with interaction of E3 with the conduction band E_c.

(smaller) compared to nominally undoped bulk ZnO crystals. The alloying of ZnO with MgO allows to predetermine the in-plane strain state of layers grown epitaxially on the AZO buffer layer. The transition from tensile in-plane strain to relaxation occurs for the samples investigated between $x = 0.5\%$ and 0.8%. The experimental results reveal distinct differences between samples with $x \leq 0.5\%$ and $x \geq 0.8\%$ that can be summarized as follows:

(i) a luminescence line Y_2 ascribed to the recombination of excitons bound to a line defect is only visible in (Mg,Zn)O thin films with $x \leq 0.5\%$. The feature is connected to tensile strain and absent in both the *c*-oriented (Mg,Zn)O films with $x \geq 0.8\%$ and the non-polar *a*-oriented ZnO film.

(ii) defects in the upper third of the (Mg,Zn)O bandgap were investigated by means of DLTS. The polar samples with $x \leq 0.5\%$ contain signatures of defects commonly observed in *c*-ZnO thin films on AZO, namely, T1, E64, E1, T2, and E3. T1, E64, and T2 are absent in relaxed *c*-oriented (Mg,Zn)O thin films with $x \geq 0.8\%$ and non-polar *a*-oriented binary ZnO samples.

(iii) the defects E3 and E3′ were investigated by using LDLTS and LR-DLTS. The structural defect E3′ is only detectable in the polar (Mg,Zn)O samples with $x \leq 0.5\%$ and therefore connected to the in-plane tensile strain within these thin films. The concentration of E3 tends to increase in (Mg,Zn)O thin films with increasing Mg-content *x* for samples with $x \geq 0.8\%$.

(iv) optical excitation using an IR-laser shows that E3 can be recharged in a (Mg,Zn)O sample with $x = 2.2\%$, while in a similar thin film with $x = 0.5\%$ (being under tensile strain) only E3′ responds to IR radiation. This indicates that the configuration of the E3 defect is sensitive to the strain state of the sample.

ACKNOWLEDGMENTS

We thank Gabriele Ramm, Holger Hochmuth, and Michael Lorenz for preparing the PLD targets and growing the samples. To Monika Hahn, who prepared the samples, we are much obliged. Furthermore, the authors are much obliged to Daniel Splith for programming a MATLAB fitting routine for the XRD data. This work was financially supported by the German Science Foundation (DFG) in the framework of SFB 762 (Functionality of Oxide Interfaces) and the Graduate School *Leipzig School of Natural Sciences*–BuildMoNa (GS185/1).

[1]S. J. Pearton, C. R. Abernathy, and F. Ren, *Gallium Nitride Processing for Electronics, Sensors and Spintronics* (Springer, 2006).
[2]R. Quay, *Gallium Nitride Electronics* (Springer, 2008).
[3]R. Bel Hadj Tahar, T. Ban, Y. Ohya, and Y. Takahashi, J. Appl. Phys. **83**, 2631 (1998).
[4]H. Kim, A. Piqué, J. S. Horwitz, H. Mattoussi, H. Murata, Z. H. Kafafi, and D. B. Chrisey, Appl. Phys. Lett. **74**, 3444 (1999).
[5]H. Kim, C. M. Gilmore, A. Piqué, J. S. Horwitz, H. Mattoussi, H. Murata, Z. H. Kafafi, and D. B. Chrisey, J. Appl. Phys. **86**, 6451 (1999).
[6]*Zinc Oxide-Bulk, Thin Films and Nanostructures*, edited by C. Jagadish and S. Pearton (Elsevier Science, 2006).
[7]H. Morkoç and Ü. Özgür, *Zinc Oxide: Fundamentals, Materials and Device Technology*, 1st ed. (Wiley-VCH, 2009).
[8]M. Grundmann, H. Frenzel, A. Lajn, M. Lorenz, F. Schein, and H. von Wenckstern, Phys. Status Solidi A **207**, 1437 (2010).
[9]H. Frenzel, A. Lajn, and M. Grundmann, Phys. Status Solidi RRL **7**, 605 (2013).
[10]M. Stölzel, A. Müller, G. Benndorf, M. Lorenz, C. Patzig, T. Höche, and M. Grundmann, Appl. Phys. Lett. **104**, 192102 (2014).
[11]V. Srikant and D. R. Clarke, J. Appl. Phys. **81**, 6357 (1997).
[12]T. Moriyama and S. Fujita, Jpn. J. Appl. Phys., Part 1 **44**, 7919 (2005).
[13]J.-M. Chauveau, D. Buell, M. Laügt, P. Vennéguès, M. Teisseire-Doninelli, S. Berard-Bergery, C. Deparis, B. Lo, B. Vinter, and C. Morhain, J. Cryst. Growth **301–302**, 366 (2007).
[14]J. Zhu, T. Aaltonen, V. Venkatachalapathy, A. Galeckas, and A. Y. Kuznetsov, J. Cryst. Growth **310**, 5020 (2008).
[15]J. Chen, H. Deng, N. Li, Y. Tian, and H. Ji, Mater. Lett. **65**, 716 (2011).
[16]S. K. Han, S.-K. Hong, J. W. Lee, J. G. Kim, M. Jeong, J. Y. Lee, S. I. Hong, J. S. Park, Y. E. Ihm, J.-S. Ha, and T. Yao, Thin Solid Films **519**, 6394 (2011).
[17]M. Brandt, H. von Wenckstern, G. Benndorf, M. Lange, C. P. Dietrich, C. Kranert, C. Sturm, R. Schmidt-Grund, H. Hochmuth, M. Lorenz, M. Grundmann, M. R. Wagner, M. Alic, C. Nenstiel, and A. Hoffmann, Phys. Rev. B **81**, 073306 (2010).
[18]M. Lorenz, H. Hochmuth, C. Grüner, H. Hilmer, A. Lajn, D. Spemann, M. Brandt, J. Zippel, R. Schmidt-Grund, H. von Wenckstern, and M. Grundmann, Laser Chem. **2010**, 140976 (2010).
[19]B. K. Meyer, H. Alves, D. M. Hofmann, W. Kriegseis, D. Forster, F. Bertram, J. Christen, A. Hoffmann, M. Straßburg, M. Dworzak, U. Haboeck, and A. V. Rodina, Phys. Status Solidi B **241**, 231 (2004).
[20]C. P. Dietrich, A. Müller, M. Stölzel, M. Lange, G. Benndorf, H. von Wenckstern, and M. Grundmann, *Bound-exciton recombination in $Mg_xZn_{1-x}O$ thin films* (Mater. Res. Soc. Symp. Proc., 2010), Vol. 1201.
[21]H. von Wenckstern, G. Biehne, R. Abdel Rahman, H. Hochmuth, M. Lorenz, and M. Grundmann, Appl. Phys. Lett. **88**, 092102 (2006).
[22]H. Kim, A. Piqué, J. Horwitz, H. Murata, Z. Kafafi, C. Gilmore, and D. Chrisey, Thin Solid Films **377–378**, 798 (2000).
[23]J. Wiff, Y. Kinemuchi, H. Kaga, C. Ito, and K. Watari, J. Eur. Ceram. Soc. **29**, 1413 (2009).
[24]A. Lajn, H. von Wenckstern, Z. Zhang, C. Czekalla, G. Biehne, J. Lenzner, H. Hochmuth, M. Lorenz, M. Grundmann, S. Wickert, C. Vogt, and R. Denecke, J. Vac. Sci. Technol., B **27**, 1769 (2009).
[25]A. Ohtomo, M. Kawasaki, T. Koida, K. Masubuchi, H. Koinuma, Y. Sakurai, Y. Yoshida, T. Yasuda, and Y. Segawa, Appl. Phys. Lett. **72**, 2466 (1998).
[26]A. Ohtomo, M. Kawasaki, I. Ohkubo, H. Koinuma, T. Yasuda, and Y. Segawa, Appl. Phys. Lett. **75**, 980 (1999).
[27]H. von Wenckstern, R. Schmidt-Grund, C. Bundesmann, A. Müller, C. P. Dietrich, M. Stölzel, M. Lange, and M. Grundmann, "The (Mg,Zn)O alloy," in *Handbook of zinc oxide and related materials: Materials* (Taylor & Francis, 2012), Vol. 1, pp. 251–313.
[28]R. Schmidt-Grund, M. Schubert, B. Rheinländer, D. Fritsch, H. Schmidt, E. Kaidashev, M. Lorenz, C. Herzinger, and M. Grundmann, Thin Solid Films **455–456**, 500 (2004).
[29]I. V. Maznichenko, A. Ernst, M. Bouhassoune, J. Henk, M. Däne, M. Lüders, P. Bruno, W. Hergert, I. Mertig, Z. Szotek, and W. M. Temmerman, Phys. Rev. B **80**, 144101 (2009).
[30]E. F. Schubert, E. O. Göbel, Y. Horikoshi, K. Ploog, and H. J. Queisser, Phys. Rev. B **30**, 813 (1984).
[31]D. G. Chtchekine, Z. C. Feng, S. J. Chua, and G. D. Gilliland, Phys. Rev. B **63**, 125211 (2001).
[32]M. Grundmann, *The Physics of Semiconductors*, 2nd ed. (Springer, 2010).
[33]C. P. Dietrich, M. Lange, G. Benndorf, J. Lenzner, M. Lorenz, and M. Grundmann, New J. Phys. **12**, 033030 (2010).
[34]A. Müller, M. Stölzel, C. Dietrich, G. Benndorf, M. Lorenz, and M. Grundmann, J. Appl. Phys. **107**, 013704 (2010).
[35]M. Grundmann and C. P. Dietrich, J. Appl. Phys. **106**, 123521 (2009).
[36]M. R. Wagner, G. Callsen, J. S. Reparaz, J.-H. Schulze, R. Kirste, M. Cobet, I. A. Ostapenko, S. Rodt, C. Nenstiel, M. Kaiser, A. Hoffmann, A. V. Rodina, M. R. Phillips, S. Lautenschläger, S. Eisermann, and B. K. Meyer, Phys. Rev. B **84**, 035313 (2011).
[37]D. V. Lang, J. Appl. Phys. **45**, 3023 (1974).
[38]A. Chantre, G. Vincent, and D. Bois, Phys. Rev. B **23**, 5335 (1981).
[39]G. Vincent, D. Bois, and A. Chantre, J. Appl. Phys. **53**, 3643 (1982).
[40]A. Y. Polyakov, I.-H. Lee, N. B. Smirnov, A. V. Govorkov, E. A. Kozhukhova, and S. J. Pearton, J. Appl. Phys. **109**, 123701 (2011).

[41]F. Schmidt, H. von Wenckstern, D. Spemann, and M. Grundmann, Appl. Phys. Lett. **101**, 012103 (2012).
[42]D. C. Look, J. W. Hemsky, and J. R. Sizelove, Phys. Rev. Lett. **82**, 2552 (1999).
[43]D. Look, C. Coşkun, B. Claflin, and G. Farlow, Physica B **340–342**, 32 (2003).
[44]D. C. Look, G. C. Farlow, P. Reunchan, S. Limpijumnong, S. B. Zhang, and K. Nordlund, Phys. Rev. Lett. **95**, 225502 (2005).
[45]H. von Wenckstern, G. Biehne, M. Lorenz, M. Grundmann, F. D. Auret, W. E. Meyer, P. J. J. van Rensburg, M. Hayes, and J. M. Nel, J. Korean Phys. Soc. **53**, 2861 (2008).
[46]F. D. Auret, S. A. Goodman, M. J. Legodi, W. E. Meyer, and D. C. Look, Appl. Phys. Lett. **80**, 1340 (2002).
[47]F. Tuomisto, K. Saarinen, D. C. Look, and G. C. Farlow, Phys. Rev. B **72**, 085206 (2005).
[48]G. Brauer, W. Anwand, W. Skorupa, J. Kuriplach, O. Melikhova, C. Moisson, H. von Wenckstern, H. Schmidt, M. Lorenz, and M. Grundmann, Phys. Rev. B **74**, 045208 (2006).
[49]H. von Wenckstern, R. Pickenhain, H. Schmidt, M. Brandt, G. Biehne, M. Lorenz, M. Grundmann, and G. Brauer, Appl. Phys. Lett. **89**, 092122 (2006).
[50]H. von Wenckstern, M. Brandt, H. Schmidt, G. Biehne, R. Pickenhain, H. Hochmuth, M. Lorenz, and M. Grundmann, Appl. Phys. A **88**, 135 (2007).
[51]F. Greuter, G. Blatter, M. Rossinelli, and F. Schmückle, Mater. Sci. Forum **10–12**, 235 (1986).
[52]A. Rohatgi, S. K. Pang, T. K. Gupta, and W. D. Straub, J. Appl. Phys. **63**, 5375 (1988).
[53]Y. Kanai, Jpn. J. Appl. Phys., Part 1 **30**, 703 (1991).
[54]J. Fan and R. Freer, J. Am. Ceram. Soc. **77**, 2663 (1994).
[55]M. Diaconu, H. Schmidt, H. Hochmuth, M. Lorenz, H. von Wenckstern, G. Biehne, D. Spemann, and M. Grundmann, Solid State Commun. **137**, 417 (2006).
[56]T. Frank, G. Pensl, R. Tena-Zaera, J. Zúñiga-Pérez, C. Martínez-Tomás, V. Muñoz-Sanjosé, T. Oshima, H. Itoh, D. Hofmann, D. Pfisterer, J. Sann, and B. Meyer, Appl. Phys. A **88**, 141 (2007).
[57]F. D. Auret, W. Meyer, P. J. van Rensburg, M. Hayes, J. Nel, H. von Wenckstern, H. Schmidt, G. Biehne, H. Hochmuth, M. Lorenz, and M. Grundmann, Physica B **401–402**, 378 (2007).
[58]Q. L. Gu, C. C. Ling, G. Brauer, W. Anwand, W. Skorupa, Y. F. Hsu, A. B. Djurisic, C. Y. Zhu, S. Fung, and L. W. Lu, Appl. Phys. Lett. **92**, 222109 (2008).
[59]M. D. McCluskey and S. J. Jokela, J. Appl. Phys. **106**, 071101 (2009).
[60]M. Schmidt, M. Ellguth, R. Karsthof, H. von Wenckstern, R. Pickenhain, M. Grundmann, G. Brauer, and F. C. C. Ling, Phys. Status Solidi B **249**, 588 (2012).
[61]W. Mtangi, M. Schmidt, F. D. Auret, W. E. Meyer, P. J. J. van Rensburg, M. Diale, J. M. Nel, A. G. M. Das, F. C. C. Ling, and A. Chawanda, J. Appl. Phys. **113**, 124502 (2013).
[62]A. Nitayama, H. Sakaki, and T. Ikoma, Jpn. J. Appl. Phys., Part 2 **19**, L743 (1980).
[63]J. C. Simpson and J. F. Cordaro, J. Appl. Phys. **63**, 1781 (1988).
[64]F. D. Auret, S. A. Goodman, M. Hayes, M. J. Legodi, H. A. van Laarhoven, and D. C. Look, Appl. Phys. Lett. **79**, 3074 (2001).
[65]J. Han, P. Mantas, and A. Senos, J. Eur. Ceram. Soc. **22**, 49 (2002).
[66]A. Y. Polyakov, N. B. Smirnov, A. V. Govorkov, E. A. Kozhukhova, V. I. Vdovin, K. Ip, M. E. Overberg, Y. W. Heo, D. P. Norton, S. J. Pearton, J. M. Zavada, and V. A. Dravin, J. Appl. Phys. **94**, 2895 (2003).
[67]C. Leach, K. Vernon-Parry, and N. Ali, J. Electroceram. **25**, 188 (2010).
[68]F. Schmidt, H. von Wenckstern, O. Breitenstein, R. Pickenhain, and M. Grundmann, Solid-State Electron. **92**, 40 (2014).
[69]L. Dobaczewski, P. Kaczor, I. D. Hawkins, and A. R. Peaker, J. Appl. Phys. **76**, 194 (1994).
[70]L. Dobaczewski, A. R. Peaker, and K. B. Nielsen, J. Appl. Phys. **96**, 4689 (2004).
[71]G. Coli and K. K. Bajaj, Appl. Phys. Lett. **78**, 2861 (2001).
[72]Y. F. Li, B. Yao, Y. M. Lu, B. H. Li, Y. Q. Gai, C. X. Cong, Z. Z. Zhang, D. X. Zhao, J. Y. Zhang, D. Z. Shen, and X. W. Fan, Appl. Phys. Lett. **92**, 192116 (2008).
[73]G. V. Rao, F. Säuberlich, and A. Klein, Appl. Phys. Lett. **87**, 032101 (2005).
[74]S. Brehme and R. Pickenhain, Phys. Status Solidi A **88**, K63 (1985).
[75]M. Schmidt, H. von Wenckstern, R. Pickenhain, and M. Grundmann, Solid-State Electron. **75**, 48 (2012).
[76]M. Schmidt, M. Ellguth, F. Schmidt, T. Lüder, H. V. Wenckstern, R. Pickenhain, M. Grundmann, G. Brauer, and W. Skorupa, Phys. Status Solidi B **247**, 1220 (2010).